Particle detection & size evaluation in solid propellant flames via experimental image analysis to improve two-phase flow simulation in rocket motors

Matthieu Nugue, Robin Devillers, Guy Le Besnerais, Nathalie Cesco

SP2016_3124722

PARTICLE DETECTION & SIZE EVALUATION IN SOLID PROPELLANT FLAMES VIA EXPERIMENTAL IMAGE ANALYSIS TO IMPROVE TWO-PHASE FLOW SIMULATION IN ROCKET MOTORS

M. Nugue[(1)], R.W.Devillers[(2)], G. Le Besnerais[(3)], N. Cesco[(4)]

(1) ONERA, Fundamental & Applied Energetics Department,
BP 80100 – 91123 Palaiseau Cedex France, Email: matthieu.nugue@onera.fr
(2) ONERA, Fundamental & Applied Energetics Department,
BP 80100 – 91123 Palaiseau Cedex France, Email: robin.devillers@onera.fr
(3) ONERA, Modeling & Information Processing Department,
BP 80100 – 91123 Palaiseau Cedex France, Email: guy.le_besnerais@onera.fr
(4) CNES, The Launcher Directorate,
52 rue Jacques Hillairet – 75612 Paris Cedex France, Email: nathalie.cesco@cnes.fr

KEYWORDS: Solid propellant, image processing, two-phase flow, size evaluation, agglomeration

ABSTRACT:

The combustion of aluminum particles is a key factor for rocket motor propulsion in terms of performance and stability. Numerical simulations is a tool enabling complex instabilities study, but input data for the two-phase models in use have an important influence on simulation results. An experimental method is used at ONERA to characterize aluminum particles at the surface of burning propellants based on shadowgraphy. A new detection method based on *"Maximally Stable Extremal Regions"* is evaluated in the present study on a test case (one propellant composition seeded with inert particles). The method shows good detection performances and more robustness compared to the previous detection method. Detection results were used to improve particles size evaluation and aggregation fraction estimation. A correction of apparent size for unfocused particles is investigated; a shape factor was used to classify particles and aggregates. The results are promising for future applications and should assist developments of accurate two-phase simulations.

1. INTRODUCTION

Solid propulsion is commonly used for space and military applications with propellants including components such as ammonium perchlorate (AP), hydroxyl-terminated polybutadiene (HTPB), and micrometer sized aluminum particles are usually seeded in proportions up to 20 wt.-%. Although aluminum powder improves ballistic performances, it has also an impact on rocket-engine stability [1, 2 and 3]. This occurs in part because aluminum droplets are not completely consumed as the flow drives them away from the surface. In order to estimate instabilities and pressure oscillations in rocket motor, two-phase flow simulation is required to account for the effects of aluminum droplets.

Therefore, aluminum particles have been the subject of many studies to develop appropriate combustion models. On the one hand, models focused on isolated droplet to determine their evaporation and combustion rates [4, 5, 6 and 7]. On the other hand several experimental set-ups have been developed to obtain accurate experimental values that can be used as inputs for two-phase flow simulations. Experimental studies have been focused on two objects classes: single particles leaving the surface (i) and agglomerates (ii):

(i) Single particles studies aim at estimating particle size and velocity which are used in two-phase flow simulations as injection conditions for the condensed phase. The parameters have a direct impact on the flow and consequently on instabilities in rocket motors. Moreover, the knowledge of particle size, not only when injected but also at each step of their combustion, provides recommendations on aluminum-droplet combustion models in agreement with experimental measurements. Two ways have been investigated for experimental measurements of aluminum droplet and alumina particles. First, particles can be captured during combustion or at the exit of test chambers with mechanical set-ups [8]. Particle size is the only parameter that can be determined this way. Second, particles can be visualized during combustion with an optical system [9, 10 and 11]. In this case, both size and velocity can be studied.

(ii) Two-phase flow losses in solid propulsion depend on size distribution of the condensed phase. During solid propellant combustion, single aluminium particles melt and can form agglomerates. Agglomerates increase the fraction number of large objects, hence increases two-phase flow losses. Because of the difficulty to evaluate agglomeration fractions and size of agglomerates with a full theoretical model for agglomeration, others approaches are reported in the literature involving geometrical analysis and correlations from experimental data [12, 13 and 14]. Experimental set-ups have also been developed to obtain measurements of agglomeration fraction and agglomerate size [15 and 16].

In order to improve the experimental characterization of both aluminium particles and agglomerates, a focusing shadowgraphy set-up has been in use at ONERA to enable particle visualization at high repetition rate (from 1 to 10 kHz) above the surface of burning propellant samples. Figure 1 shows an example of image obtained with the ONERA set-up for an aluminized propellant. The propellant surface corresponds to the black region at the bottom of the image. Aluminum particles leave the propellant and move up driven by the combustion-gas flow. Particle detection on the image is hindered by smokes that disturb the homogeneity of the background image. The existing detection method at ONERA consisted of filters and segmentation with manual intensity thresholds. This approach has been used in previous works [9, 10 and 11] and provided particle granulometry and a limited number of velocity profiles. However, it relied on several human interventions: about half a dozen parameters were adjusted manually to improve the detection process, and a set of a dozen morphological properties needed to be tuned before validating the detected objects. Thus this method could not be used smoothing to obtain a large set of data, required for the statistical estimation of particles characteristics.

In the present study, we propose a new image processing method in order to automatically detect and characterize aluminum particles in burning propellant atmospheres with a more efficient and robust way, reducing the number of input parameters. In this preliminary work, we aim at evaluating the proposed method on test cases, with a representative propellant atmosphere but seeded with inert particles.

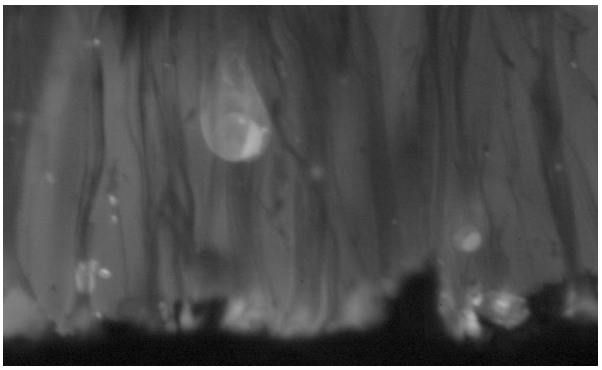

Figure 1. Shadowgraphy image near the burning surface of an aluminized propellant.

2. MATERIALS AND METHODS

The validation of the image analysis method is performed on experimental images for a propellant seeded with inert particles (glass-type particles) of calibrated size (6 wt. %) instead of aluminum particles. Thus the visualization is not disturbed by aluminum smokes and particles size is not impacted by combustion during the

experiment. Moreover, the size distribution of inert particles was evaluated with laser-diffraction analyzer before their inclusion in the propellant and will be used as a reference granulometry data. Examples of experimental images are presented in Figure 2 for the two pressures used for combustion tests (1 MPa and 3 MPa). The pressure levels correspond to the initial pressure in the combustion chamber, filled with pure nitrogen before propellant ignition. Figure 2 a) at 1 MPa shows images without visible smokes and with clearly-contrasted particles driven by the flow. On Figure 2 b) at 3 MPa, aggregates of single inert particles are driven by the flow in addition to single particles. The pressure increase leads to steeper optical index gradients and visible background heterogeneities.

2.1. Particle detection

To detect the inert particles leaving the propellant surface, we used the Maximally Stable Extremal Regions (MSER) method introduced in [17]. MSER detection has been proposed in the context of feature matching between images in computer vision. The principle of MSER is illustrated in Figure 3 on an experimental image of the studied propellant.

The basic operation in MSER is to binarize the image according to various threshold levels. As shown in Figure 3, this operation is repeated for increasing values of the threshold. The main idea of MSER is then to retain the regions whose shape is stable (*i.e.* the size variation of the region does not exceed an input parameter, denoted MaxVariation) over a range of threshold values (the "stability parameter" denoted Δ). Therefore, MSER enables detections of small and large objects with opposite contrast and variable shape, which is useful in our case to detect complex aggregates as well as single particles.

A low-pass filter is employed to reduce acquisition noise and the associated spurious detection of small regions with area around 6 px. One minor consequence of such image filtering is to increase the size of MSER regions. The number of parameters of the detection process has been drastically reduced which permits to propose a more principled way of tuning them.

2.2. Evaluation of detection performance

To evaluate the performance of the MSER detector and guide the tuning of parameters, results from automated detections of regions (particles) were compared with a ground truth established by manually spotting the real particles on a set of images. Such comparisons lead to three possibilities: True Positive (TP) or detection of a true particle; False Positive (FP) or erroneous detection of a "ghost" particle and False Negative (FN), which means that a true particle is missed by the algorithm. Because it is necessary to both detect and localize all particles in the image, the problem is not binary (contrary to a pure detection problem). This is a well-known issue in image processing, and two useful performance indexes have been introduced:

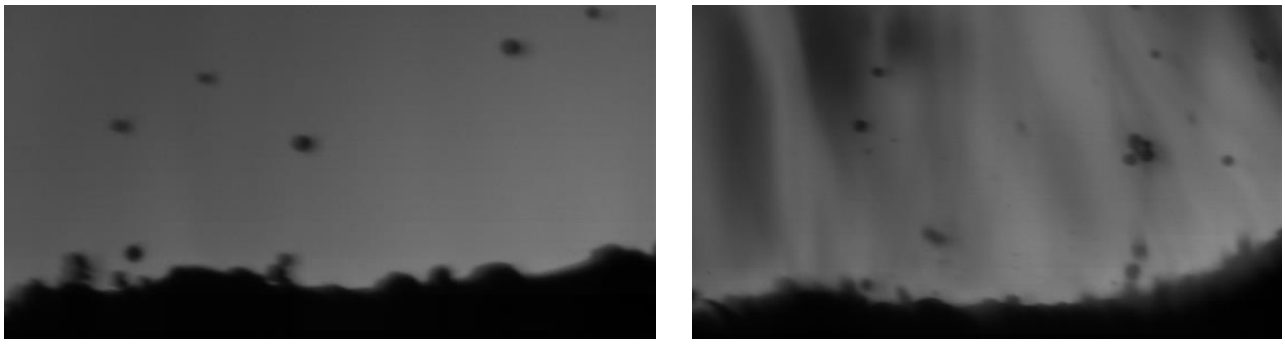

a) Initial Pressure: 1 MPa *b) Initial Pressure: 3 MPa*

Figure 2. Shadowgraphy images of the burning surface of a propellant seeded with inert particles at 1 MPa (a) and 3 MPa (b).

- *Recall* characterizes the completeness of the detection: Recall = 1 means no real particle has been missed.

$$Recall = \frac{TP}{TP + FN} \quad (1)$$

- *Precision* characterizes the relevance of detection: Precision = 1 means that there is no ghost particle in the detected set.

$$Precision = \frac{TP}{TP + FP} \quad (2)$$

Usually, the detection depends on some tuning parameter, which is tuned according to a Precision vs. Recall curve. This is the approach that was adopted here with the parameter Δ for the MSER detector, see Section 3.1.

In order to prevent multiple detections of the same particle in consecutive images, the detection is performed in a horizontal region above the propellant surface. The height of this region must be large enough to detect all particles, and narrow enough to prevent multiple detections. The size of the detection zone is computed in the worst case, i.e. when particles are the slowest (at 1 MPa and close to the propellant surface). Previous works conducted at ONERA [9] have estimated the velocity of particles close to the surface at 0.5 m/s for the same propellant composition. The probing height was then evaluated considering the camera repetition rate (3 kHz).

2.3. Size evaluation

To estimate the diameter of detected particles, we use the area of the detected MSER regions (A_{MSER}) and determine the Equivalent-Area Circle's diameter (D_{EAC}) based on the equivalent circular area [18], given by Eq. 3:

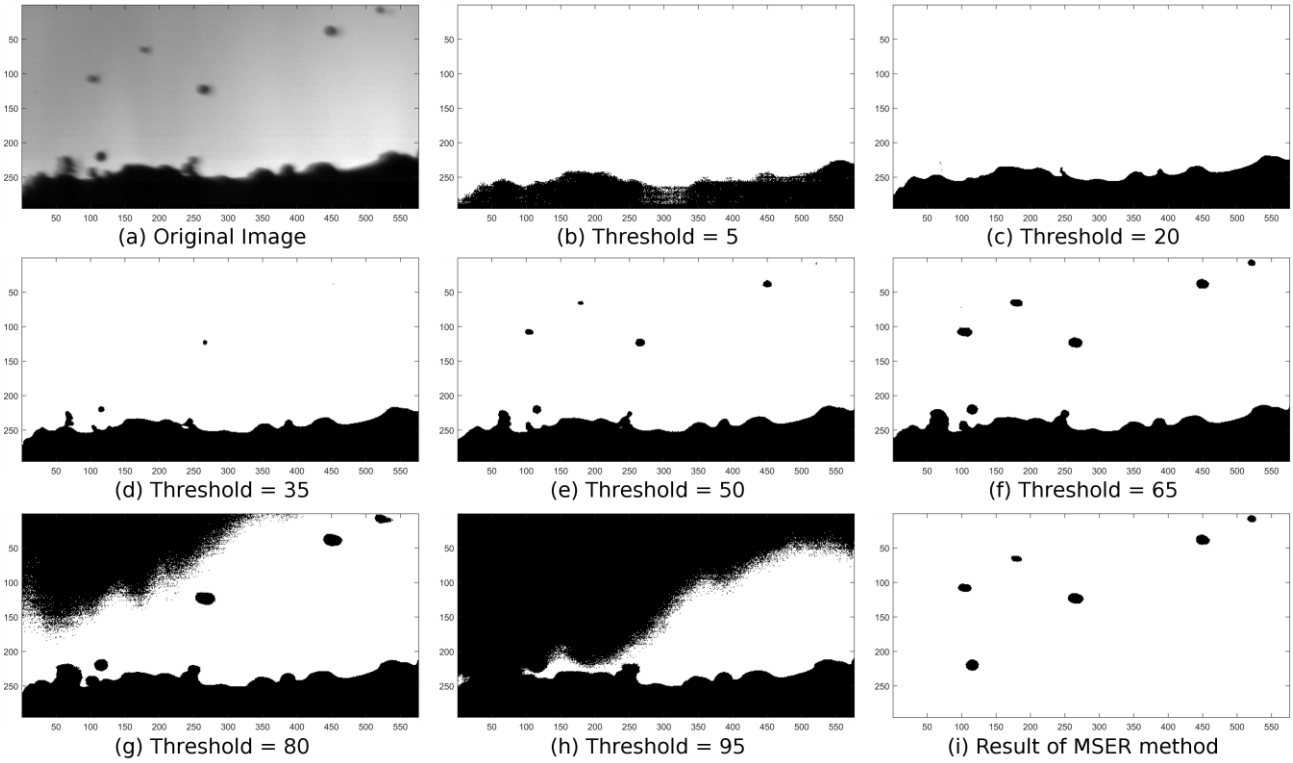

Figure 3. Principle of MSER: the experimental image (a) is binarized according to increasing threshold values. Regions that are stable for a large range of thresholds are retained (results in (i)).

$$D_{EAC} = C\sqrt{\frac{4A_{MSER}}{\pi}} \quad (3)$$

This approach makes sizing of non-spherical particles (aggregates) possible, as shown in Figure 4.

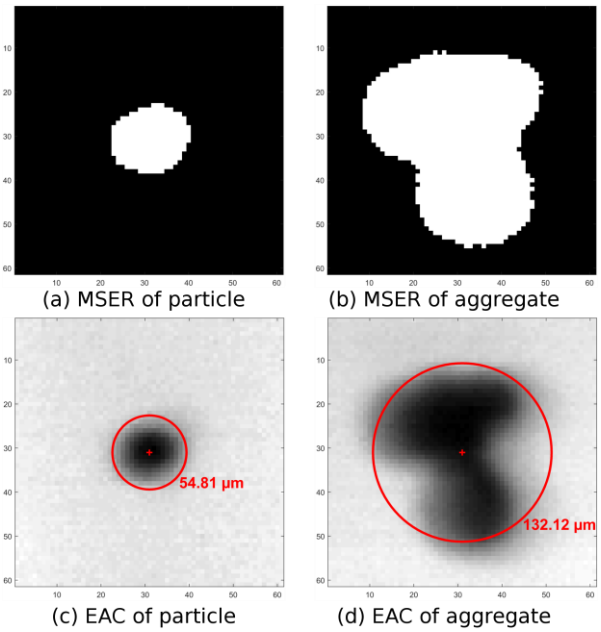

Figure 4. Particle-size evaluation. Picture (a) shows the MSER result for a particle, and picture (b) shows the MSER result for an aggregate. Pictures (c) and (d) show red circles of D_{EAC} for (a) and (b) respectively, overlaying the initial shadowgraphy image.

It is important to underline the likely overvaluation of A_{MSER}, because images of the particles are generally out of focus in shadowgraphy. More precisely, the further a particle is from the focus plane, the more spread its shadowgraphy image is. Deconvolution of defocused particles is widely studied in the literature [19 and 20], however this approach can be limited by noise amplification. A correction of the apparent diameter for out-of-focus particles was established in [21] and its main principles were used in the present study. The method consists in creating a theoretical imaging model based on the irradiance distribution of the object and the Point Spread Function of the imaging system. This model is used to determinate the relationship between in-focus radius and the measured apparent radius of the object according to experimental image parameters, e.g. the relative detection threshold and a normalized contrast (contrast between the object and the background). Determination of the normalized contrast and the detection threshold for each particle leads to the corrected diameter via interpolation plots obtained from the imaging model.

The relevance of the full imaging model from [21] was not checked for the present experimental shadowgraphy set-up, so the correction accuracy is probably perfectible. Nevertheless, the correction interpolations from the publication were used to obtain a rough estimate of the expected diameter correction for the MSER detection, by calculating their normalized contrast and detection threshold.

2.4. Aggregation evaluation

As stated earlier, predicting particle agglomeration remains an ongoing task for propellant studies, and shadowgraphy images might provide interesting data on this aspect. In the case of aluminized-propellant combustion, agglomerations phenomena are the consequence of assembled droplets that melt to create an agglomerate (i.e. a single droplet with a size bigger than initial droplets). In the present study, particles are inert and do not melt to create agglomerates but they might form aggregates. In order to classify particles and aggregates, a score has been computed for each MSER. Following [22], we rely on shape factors to classify the objects. The chosen shape factor quantifies the roundness of an object. The circularity given by Eq. 4 compares the area of MSER to its perimeter P. Circularity is bounded by 0 for a perfect line and 1 for a perfect circle.

$$Circularity = \frac{4\pi A_{Poly}}{P^2} \quad (4)$$

P is the polygon length defined on the boundaries pixels of the detected MSER region. The area of this polygon (A_{Poly}) is smaller than A_{MSER} but more representative of the exact included area.

3. RESULTS

3.1. Detection performance

MaxVariation and Δ are the two main parameters of MSER detection, and they are obviously coupled. As shadowgraphy images are not only blurred, but show a variable blur level depending on the position of the particle, it is difficult to tune the MaxVariation. Hence we choose a fixed value (MaxVariation = 1) for this parameter and perform the parametric study on Δ. This study relies on Precision vs. Recall curves. The chosen value of MaxVariation enables to detect regions with maximum diameter variation equal to 40 % over the range of Δ values.

Figure 5 represents the Precision-Recall curves for propellant seeded with inert particles for the two combustion pressures: 1 MPa (red solid line) and 3 MPa (blue dash line). The MSER detection method was compared to manual detection for 200 images (corresponding to around 500 particles). Figure 5 displays the values of Δ next to each data point. Choosing Δ amounts to selecting the best trade-off between Precision and Recall, i.e. a point as close as 100 % for both Recall and Precision. Thus, we have chosen Δ = 8 at 1 MPa and Δ = 4 at 3 MPa in the sequel. One can note that the test at 3 MPa has a lower Precision for all tested Δ values in comparison with the test at 1 MPa. Indeed, higher pressure increases the density gradient between smokes and flow and, as a consequence, the contrast of smokes increases and degrades the detection. To conclude, the chosen MSER parameters (MaxVariation and Δ) lead to at least 90 % for the Recall and 80 % for the Precision.

As a comparison, Precision and Recall values were calculated for existing detection data obtained with the previous existing processing method, over a wide range of combustion conditions (aluminum-seeded propellants with various size distribution, various test pressures…). The cautious adjustment of the numerous input parameters lead to Precision over 80%, but Recall could range from 30% to 90% (visible on Figure 5 as square symbols). The proposed method should provide more stable performances than previously with a much more automated tuning process (Δ was the single input parameter adjusted for MSER).

3.2. Size evaluation

As stated earlier, inert particles were characterized with a laser-diffraction analyzer before preparing the propellant material. The resulting distribution of size was used as a reference for particle-size evaluation from the experimental images. The detection method has been used on 1000 images per test (e.g. around 2000 particles detected per test) to obtain the D_{EAC} distribution. Figure 6 shows the comparison between the reference size distributions using laser-diffraction analyzer (black dashed line) and image analysis at 1 MPa (red plot) and 3 MPa (blue plot).

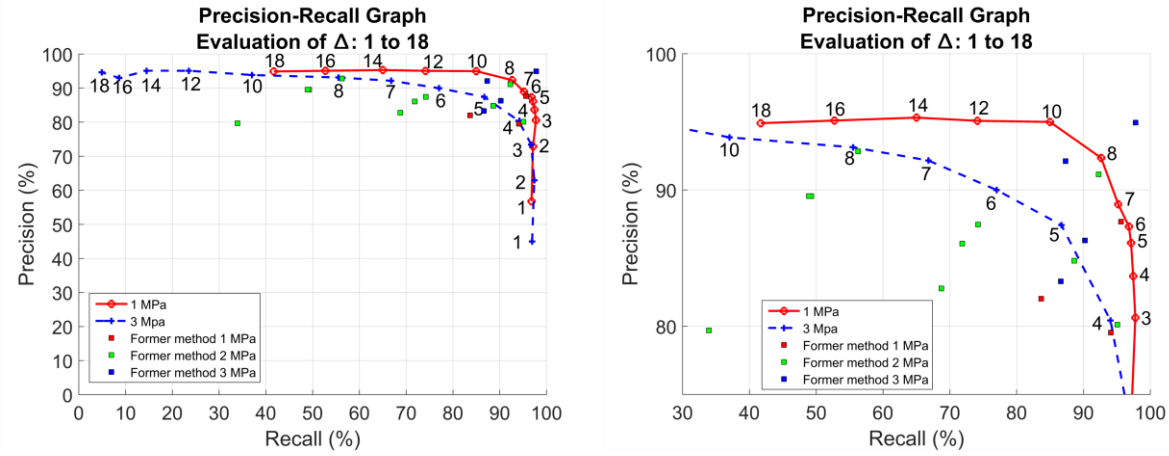

Figure 5. Precision-Recall graph: Evaluation of Δ (close up on the right-hand side). Comparison with values using the previous image-processing method (square symbols).

A shift is visible between peaks for the reference distribution and the estimated one. This shift can be explained by overvaluation of the area estimated from MSER regions due to out-of-focus particles. Additional detections are visible for diameters around 10 µm for both image-analysis curves. They seem to be caused by an image noise that is not removed by the mean filter. Designing an image processing to reduce the number of such spurious detections on experimental images is the subject of future works. Peaks for diameter 80 µm seem to correspond to aggregates because such particle size is not present in the initial lognormal distribution provided by the reference granulometry. Moreover, the larger aggregate proportion at 1 MPa compared to 3 MPa is consistent with the expected behaviour for propellant combustion [13].

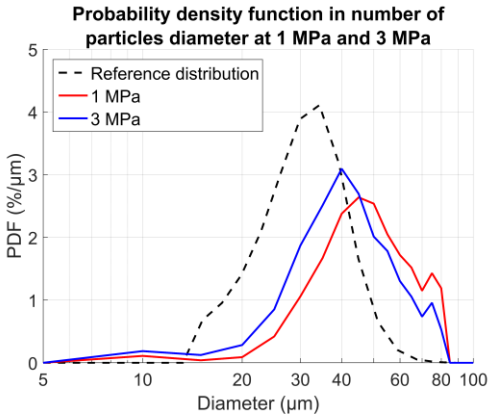

Figure 6. Particle size distribution measured with image analysis at 1 MPa and 3 MPa, as well as reference distribution for the initial inert particles.

As mentioned in Section 2.3, a correction of the apparent diameter has been computed for each particle at 1 MPa and 3 MPa in order to account for focus conditions, based on the method from [21].

Figure 7 displays size distributions for the reference granulometry (black dashed line), for D_{EAC} before diameter correction (red and blue dashed lines) and after correction (red and blue solid lines, labeled D_{COR}). For 1 MPa data and diameter below 70 µm, the diameter correction appears efficient and lead to a very good fit of the distribution estimated from the images and the reference ones. In contrast, the distributions of particle diameters below 70 µm at 3 MPa are not significantly impacted by the correction. This might be due to the different imaging conditions at 3 MPa and limits of the imaging model from [21] for such conditions. Finally, let us note that for both conditions the correction method leads to an increase of the estimated diameter of particles which diameters are over 70 µm up to 120 µm. Actually, this diameter range is likely to correspond to aggregates and the correction is not valid for non-spherical objects. To conclude, precise diameter estimation will need improvements in the future via a complete study of the shadowgraphy set-up.

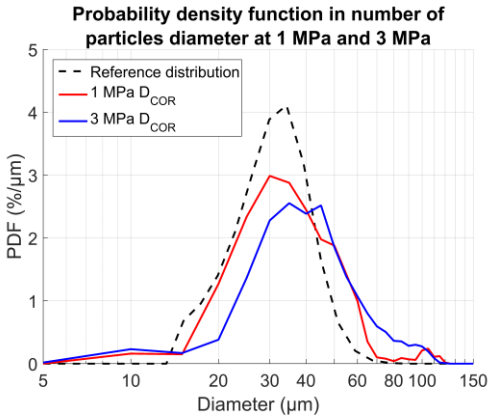

Figure 7. Particles size distribution after correction of out of focus effect [21].

3.3. Aggregation

A simple approach to evaluate the aggregation fraction could be to use the maximum diameter from the reference distribution as a ceiling value (any larger object cannot be considered as a single particle). Unfortunately this method does not discriminate aggregation of small particles leading to aggregates smaller than the diameter chosen as threshold. As explained before, the circularity parameter was used to discriminate round particles from aggregates. Figure 8 shows a 2D histogram of the diameter and circularity of detected particles for each tested pressure.

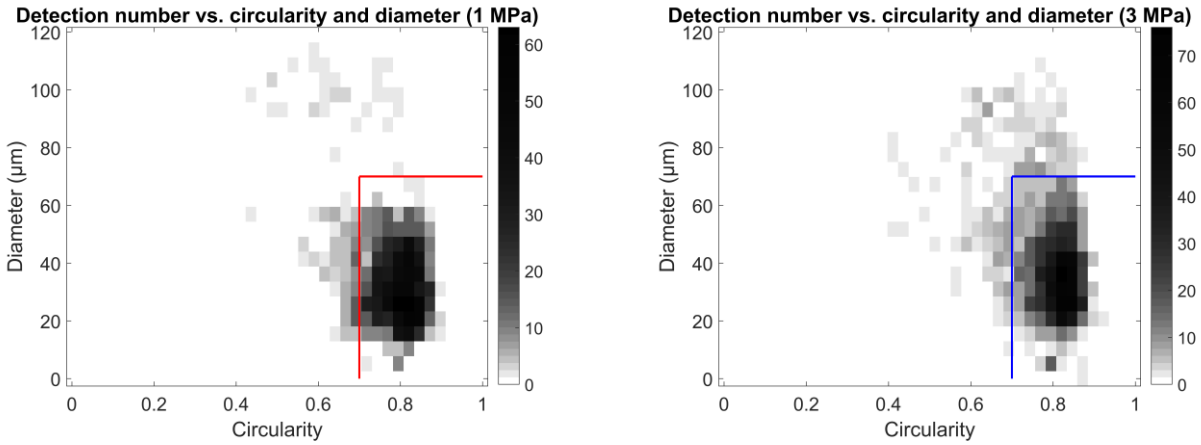

a) Initial Pressure: 1 MPa *b) Initial Pressure: 3 MPa*

Figure 8. 2D histograms of circularity and diameter of the detected particles at 1 MPa (a) and 3 MPa (b) .

There is an important concentration of detections for circularities equal to 0.8 and a decrease of detections for circularity below 0.7. The circularity 0.7 appears as a relevant value to separate single particles from aggregates. As an illustration, some examples of detected objects are shown for various circularity values in Figure 9.

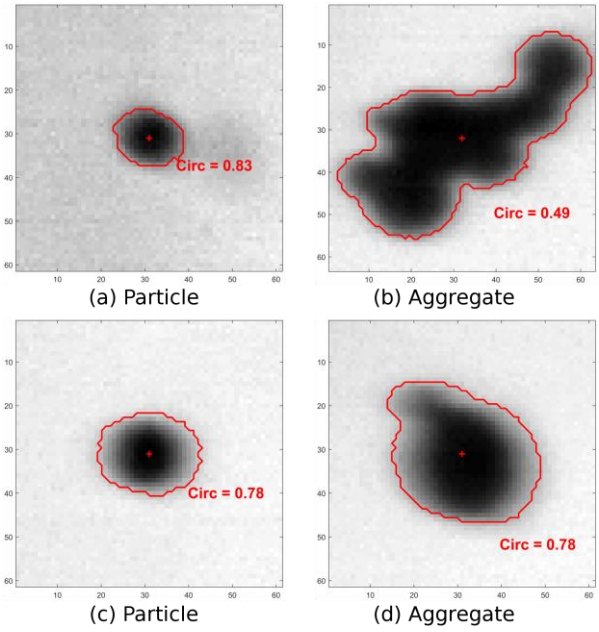

Figure 9. Objects detected with MSER and the associated circularity.

Additionally, the biggest diameter for the reference distribution is used as a ceiling value for diameter (70 µm). Larger detected objects are considered aggregates over the full circularity range. The single-particle regions correspond to the lower-right corner on the histograms of Figure 8. Very large aggregates can be formed of a large number of particles that can be seen as a dense, almost round pack on the image, as illustrated in the lower right image of Figure 9. Circularity alone would not be efficient in such cases.

With those criteria, a rough estimation of aggregation fraction was computed: around 50 wt.-% for the test at 1 MPa and around 60 wt.-% at 3 MPa. These estimates seem overvalued compared to visual checking on the images. Moreover, an indicative comparison was performed with the aluminum agglomeration correlations summarized in [12]. The correlations were used to get a rough estimate of agglomeration fraction for the same propellant seeded with aluminum particles instead of inert particles (e.g. with the same AP granulometry). Obviously, such correlations depend on material properties for the analysed particles, such as melting levels, which makes it impossible to expect accurate results with the present inert particles. Still, they provide an indication to critically analyse our approach. The Beckstead correlation gives an agglomeration fraction around 17 wt.-% and the Cohen correlation evaluate aluminum agglomeration around 33 wt.-%. Both values are significantly lower than the fractions which were estimated here.

A deeper analysis can explain this difference. It seems likely that the calculated volume is overestimated for aggregates because it assumes a spherical geometry for the objects, whereas

aggregates can be planar arrays of particles since inert particles do not melt. To estimate the volume under a planar assumption the mean diameter of a single particle was used to evaluate the number of particles that could be included in the apparent area of aggregates. This corresponds to a lower value of the estimated volume since aggregates are usually non exactly planar. The two assumptions are represented schematically on Figure 10.

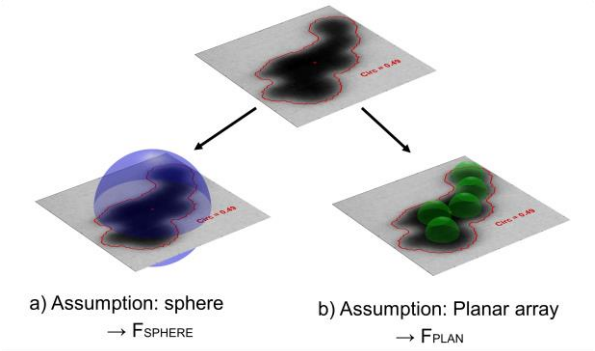

Figure 10. Volume estimation for aggregates with a spherical or planar assumtion.

Figure 11 displays agglomeration fraction for Cohen correlation (black solid line), Beckstead correlation (black dashed line), aggregation fraction computed under the spherical geometry assumption for aggregates (denoted F_{SPHERE}) and aggregation fraction under the planar assumption (denoted F_{PLAN}). In the case of F_{PLAN}, the estimated volume obviously depends on the assumed size of the particles, which follows the distribution identified in Section 3.2. We retain the mean value and standard deviation of this distribution to draw the error bars on the aggregation fraction F_{PLAN} represented in Figure 11. F_{PLAN} estimation provides a reasonable estimate for aggregation fraction.

These results show that, with a more systematic and accurate estimation of aggregation volumes, shadowgraphy image analysis for inert-particle propellants could be an interesting way to validate aluminum agglomeration models.

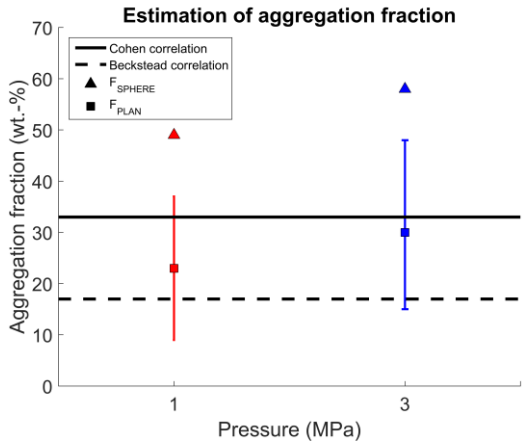

Figure 11. Estimation of aggregation fraction for the two assumption on aggregate's geometry. Agglomeration fractions from published correlations [12] are also displayed.

4. CONCLUSION & DISCUSSION

The purpose of this paper was to propose an automated method for particles detection and size evaluation in solid propellant flames up to 3 MPa. Validation was conducted on a test-case propellant seeded with inert particles.

The detection method is based on MSER. It leads to 90 % for the Recall and 80 % for the Precision. Recall is better and more stable compared to the previous analysis method, whose Recall values could range from 40% to 90% depending on the test conditions. Comparison between reference size distribution (from laser-diffraction analyzer) and size distribution evaluated on detected particles was performed. Defocus blur leads to overestimation and a diameter correction was tested. Result of the diameter correction depends of the test conditions and size of detected regions. The method appears promising, but should be improved via a complete characterization of the shadowgraphy set-up.

We have also presented a preliminary approach to evaluate aggregation fraction by classification of detected objects between single particles and aggegates. The rough estimate of the aggregation fraction is consistent with aluminium-agglomeration correlations calculated for propellants with the same AP granulometry. Advanced techniques of object classification seem

to be an interesting line of research to improve the determination of the aggregation fraction. This should enable accurate comparison to model prediction for real combustion conditions.

Future work concerns the tracking of detected particles on sequences of images. Tracking and monitoring particle's shape within the sequence will give access to particles velocity, ignition height and variations of the aluminium-particle diameter at several heights and provide valuable data for model development.

More generally, exchanges between models and experimental data analysis are in our opinion of major interest to improve rocket-flow predictions. Before full-scale simulation, performing simulations for combustion chamber used for shadowgraphy measurements will be an appropriate intermediate step. In this line, we intend to conduct two-phase flow simulations with the same propellant composition used in experimental analysis.

5. ACKNOWLEDGEMENTS

The work presented in this paper is part of a CNES/ONERA PhD thesis.

6. REFERENCES

1. Guéry, J.F., Ballereau, S., Godfroy, F., Gallier, S., Orlandi, O., Della Pieta, P., Robert, E. & Cesco, N. (2008). Thrust Oscillations in Solid Motors. In Proc. 44th AIAA, 2008-4979.

2. Gallier, S. & Godfroy, F. (2009). Aluminum Combustion Driven Instabilities in Solid Rocket Motors. *Journal of Propulsion and Power*, Vol. 25, No 2.

3. Casalis, G., Boyer, G. & Radenac, E. (2011). Some recent advances in the instabilities occurring in long Solid Rocket Motors. In Proc. 47th AIAA, 2011-5642.

4. Law, C.K. (1982). Recent advances in droplet vaporization and combustion. *Prog. Energy Combust. Sci.*, Vol. 8, pp. 171-201.

5. Daniel, E. (2000). Eulerian Approach for Unsteady Two-Phase Solid Rocket Flows with Aluminum Particles. *Journal of Propulsion and Power*, Vol. 16, No. 2.

6. Beckstead, M.W. (2004). A Summary of Aluminum Combustion. In *Internal Aerodynamics in Solid Rocket Propulsion*, RTO/NATO EN-023(5).

7. Fabignon, Y., Orlandi, O., Trubert, J.F., Lambert, D. & Dupays, J. (2003). Combustion of aluminum particles in solid rocket motors. In Proc. 39th AIAA, 2003-4807.

8. Gallier, S. & Yiao, M. (2013) Aluminum agglomeration model calibration with improved experimental data. *Journal of Propulsion and Power*, Vol. 29, No 5, pp.1252-1255.

9. Cauty, F. & Erades, C. (2012). Tracking of aluminum particles burning in solid propellant combustion gases by focusing schlieren technique. In Proc. 15th International Symposium on Flow Visualization.

10. Devillers, R.W., Erades, C., Lambert, D. & Bellessa, J. (2014). Mesure et suivi de particules, agglomérats et gouttes en combustion au dessus de la surface d'un propergol en combustion. 14th CFTL, Marseille, 15-19 September (In French)

11. Liu, X., Peiji, L. & Bingning, J. (2015). Experimental Study on Combustion of Aluminum in Composite Propellant. In Proc. 51st AIAA, 2015-3977.

12. Gallier, S., (2009). A Stochastic Pocket model for Aluminum Agglomeration in Solid Propellants. *Propellants Explos. Pyrotech.*, Vol. 34(2), pp. 97-105.

13. Yavor, Y., Gany, A. & Beckstead, M.W. (2014). Modeling of the Agglomeration Phenomena in Combustion of Aluminized Composite Solid Propellant. *Propellants Explos. Pyrotech.*, Vol. 39, pp. 108-116.

14. Maggi, F. & DeLuca, L.T. (2015). Pocket model for aluminium agglomeration based in propellant microstructure. *AIAA Journal*, Vol. 53, No. 11, pp. 3395-3403.

15. Trubert, J.F. (2000). Agglomeration and combustion of aluminium particles in solid rocket motors. 2nd European Conference on Launcher Technology, Space Solid Propulsion, Paper 44.

16. Sippel, T.R., Son, S.F. & Groven, L.J. (2014). Aluminum agglomeration reduction in a composite propellant using tailored Al/PTFE particles. *Combustion and Flame*, Vol. 161, pp. 311-321.

17. Matas, J., Chum, O., Urban, M. & Pajdla, T. (2002). Robust Wide Baseline Stereo from Maximally Stable Extremal Regions. In Proc. British Machine Vision Conference, Vol. 22(10), pp 761-767.

18. Kashdan, J.T., Shrimpton, J.S. & Whyrew, A. (2003). Two-Phase Flow Characterization by Automated Digital Image Analysis. Part 1: Fundamental Principles and Calibration of the Technique. *Part. Part. Syst. Charact.*, Vol. 20, pp. 387-397.

19. Kim, I.G. & Lee, S.Y. (1990). A simple Technique for Sizing and Counting Spray Drops Using Digital Image Processing. *Experimental Thermal Fluid Science*, Vol. 3, pp. 214-221.

20. Fantini, E., Tognotti, L. & Tonazzini, A. (1990). Drop Size Distribution in Sprays by Image Processing. *Computers Chem. Engng.*, Vol. 14(11), pp. 1201-1211.

21. Blaisot, J.B. & Yon, J. (2005). Droplet size and morphology characterization for dense sprays by image processing: application to the Diesel spray. *Experiments in Fluids*, Vol. 39, pp. 977-994.

22. Chigier, N. (1991). Optical Imaging of Sprays. *Prog. Energy Combustion Science*, Vol. 17, pp. 211-262.